RSC Advances

PAPER

View Article Online
View Journal | View Issue

Cite this: *RSC Adv.*, 2024, **14**, 9860

Aqueous exfoliation and dispersion of monolayer and bilayer graphene from graphite using sulfated cellulose nanofibrils

Benjamin Pingrey,[a] James D. Ede,[b] Christie M. Sayes,[c] Jo Anne Shatkin,[b] Nicole Stark[d] and You-Lo Hsieh *[a]

Received 16th January 2024
Accepted 14th March 2024

DOI: 10.1039/d4ra00424h

rsc.li/rsc-advances

Amphiphilic sulfated cellulose nanofibrils were synthesized with yields in excess of 99% by sulfation of dissolving pulp cellulose using chlorosulfonic acid in anhydrous *N*,*N*-dimethyl formamide followed by high-speed blending. The sulfation level was stoichiometrically tunable to between 1.48 and 2.23 mmol g^{-1}. The optimized SCNF demonstrated the ability to act as an effective dispersant for graphene produced *via* exfoliation in aqueous media, allowing for the production of aqueous stabilized graphene with 3.9 ± 0.3 wt% graphite to graphene conversion and suspended solids comprised of 19.5 ± 1.5 wt% graphene. Graphene exfoliated with SCNF was observed to consist exclusively of mono- and bilayers, with 42% of sheets being monolayer. Furthermore, it was demonstrated that SCNF defibrillation and graphene exfoliation could be combined into a single one-pot process.

Introduction

Graphene, consisting of single layers of sp^2 hybridized carbon atoms arranged in a hexagonal lattice structure, exhibits impressive electrical, thermal, and mechanical properties that have led to intensive interest since its discovery in 2004. Graphene has a high electron carrier mobility of up to 200 000 $cm^2 V^{-1} s^{-1}$, giving rise to a correspondingly high in-plane electrical conductivity.[1] The thermal conductivity of graphene is on the order of 3000 W $m^{-1} K^{-1}$; nearly an order of magnitude higher than that of copper.[1] Monolayers of graphene possess a staggeringly high tensile modulus of 1 TPa, making it among the strongest materials ever measured.[2] Despite these outstanding properties, graphene has yet seen widespread adoption, largely due to the difficulty of producing high quality graphene in monolayers consistently and in bulk.[3]

The simplest way to produce graphene sheets is by peeling them off of graphite using cellophane tape;[1] a simple top-down mechanical method that produces some of the highest quality graphene sheets available. However, this method is neither high-yielding nor scalable, and is therefore nonviable for any form of bulk production. Alternative top-down mechanical shearing approaches have mainly involved liquid exfoliation of graphite or graphite oxide in organic[4–6] or aqueous[7–10] media. Graphite has been converted into graphite oxide and then ultrasonicated in *N*,*N*-dimethylformamide (DMF) into graphene oxide and subsequently reduced into graphene using hydrazine.[10] Direct exfoliation of graphite *via* shearing is possible in organic liquids with surface energies close to that of graphene (*ca.* 70–80 mJ m^{-2}),[6] including DMF,[11] *N*-methyl-2-pyrrolidone (NMP),[5] and 1,2-dichloroethane.[4] While these organic liquid exfoliation processes aid the dispersion of graphene, the use of organic solvents imposes hazards as well as additional processing steps and costs. In order to aqueously exfoliate graphite, the use of dispersants, such as poly(styrene sulfonate),[7] porphyrins,[8] sodium salts,[9] and 1-pyrenebutyrate,[10] is necessary to suspend graphene in water. These dispersants act by building up electrical double layers on graphene surfaces. In the cases of mono- or even few-layer graphene, the presence of significant quantities of dispersants is necessary, leading to low graphene concentration and a dramatic reduction in the conductivity of the resulting product. As an example, an aqueous dispersion of graphene containing 1-pyrenebutyrate was stable at a concentration of 0.1 mg mL^{-1}, but yielded a low in-plane conductivity of only 2 S cm^{-1}.[10]

We previously demonstrated that C6 carboxylated cellulose nanofibrils (CNFs) produced through TEMPO-mediated oxidation of rice straw cellulose coupled with high-speed blending[12] were effective in facilitating the exfoliation of graphite into graphene and stabilize the resulting graphene at concentrations of up to 1 mg mL^{-1}, all in aqueous media.[13] The effectiveness of the TEMPO CNF was postulated to be a result of amphiphilicity on the nanofibrillar surfaces. The hydrophobic (200) crystalline planes of TEMPO CNF faced with carbon and axial hydrogen atoms could associate with graphene surfaces, acting similarly

[a]*Biological and Agricultural Engineering, Chemical Engineering, University of California at Davis, Davis, CA 95616-8722, USA. E-mail: ylhsieh@ucdavis.edu; Tel: +1 530 752 0843*
[b]*Vireo Advisors, LLC, PO Box 51368, Boston, MA, 02130, USA*
[c]*Environmental Science, Baylor University, Waco, TX 76798-7266, USA*
[d]*USDA Forest Service, Forest Products Laboratory, Madison, WI 53726-2398, USA*

to cellophane tape used during manual exfoliation and helping with the shear force applied during blending to peel off graphene. Simultaneously, the nanocellulose's surface hydrophilic hydroxyl groups and charged carboxylates present on (110) planes allow hydrogen bonding to water and dispersing graphene as stable aqueous dispersions.

Although TEMPO CNF were effective in aiding exfoliation and dispersing the exfoliated graphene, the high cost of TEMPO itself raises the need for alternative nanocelluloses, given the diversity of cellulose chemistry and the potential effectiveness in facilitating graphene production. Of particular interest are sulfated nanocelluloses, which are both anionic like TEMPO CNF and can be easily produced through multiple sulfation routes. Sulfation of cellulose has been known for decades to produce water dispersibility and super absorbency imparted by hydrophilic sulfate groups.[14] Aqueous sulfation of various craft pulps,[15,16] cotton,[17] and CNCs[18] with sodium metaperiodate and sodium bisulfite has produced macroscopic sized sulfated cellulose,[15,17] 10–60 nm wide CNF,[16] and 200–300 nm diameter spheres or 8 nm wide CNCs.[18] Sulfation of freeze-dried CNF[19] and cellulose powder[20] with chlorosulfonic acid in DMF, on the other hand, produced sulfated CNF with less than 100 nm diameters[19] or soluble sulfated cellulose.[20] Sulfation of pulp cellulose with sulfamic acid and urea as a deep eutectic solvent generated 4 nm wide CNF, however, some extent carbamation was observed due to the use of urea.[21] We previously established a straightforward and robust procedure for the direct production of sulfated cellulose nanofibrils (SCNF) from macroscale rice straw cellulose using chlorosulfonic acid in DMF followed by high-speed blending, to convert 94–97% cellulose into SCNF.[22] These SCNF displayed evidence of amphiphilic surface behavior, analogous to TEMPO CNF, while possessing a wider range of tunable charges, ranging from 1.0 to 2.2 mmol of sulfate half-ester groups per gram of SCNF.

The current work aims to explore the stoichiometrically optimized sulfation of the most abundantly available cellulose feedstock, *i.e.*, dissolving pulp, into SCNFs and the efficacy of SCNF for exfoliating and dispersing graphene in comparison to that of the TEMPO CNF demonstrated previously. The relationship between the sulfation levels of SCNFs and the exfoliation efficacy of graphite into graphene was examined by optimizing exfoliation conditions with mechanical blending to maximize graphene production. The effectiveness of SCNF at exfoliating graphite into graphene, the dimensions of graphene sheets, and the conductivity of films formed by vacuum filtration of aqueous graphene dispersions were assessed. Additionally, streamlining the defibrillation of sulfated cellulose into SCNF and the exfoliation of graphite to graphene by combining these two separate processes into one single, simultaneous blending step was investigated to reduce the total time and energy input for this aqueous exfoliation approach.

Experimental

Materials

Anhydrous *N*,*N*-dimethylformamide (DMF) and graphite flakes (~50 μm thickness) were obtained from Sigma-Aldrich (Burlington, MA, USA). Sodium hydroxide (1.00 N) solution was obtained from Spectrum Chemical (New Brunswick, NJ, USA). Chlorosulfonic acid (HSO_3Cl, 99%) was obtained from Alfa Aesar (Ward Hill, MA, USA). Softwood dissolving pulp cellulose sheets were received from the Forest Product Laboratory of the United States Department of Agriculture Forest Service in Madison, WI, USA. Ultra-pure water was acquired from a Milli-Q Advantage A10 water purification system. Regenerated cellulose dialysis tubing (12–14 kDa molecular weight cutoff) and polycarbonate filters (47 mm diameter, 0.6 μm pores) were purchased from Spectrum Laboratories (San Francisco, CA, USA). Dowex Marathon C (H-form) acidic ion exchange resin beads were purchased from Fisher Scientific (Waltham, MA, USA). Unless otherwise noted, all materials were used as-is.

Synthesis of sulfated cellulose nanofibrils

Sulfated cellulose nanofibrils were synthesized from dissolving pulp cellulose following a previously reported procedure.[22] In brief, sheets of dissolving pulp cellulose (1 g) were torn into small squares circa 1 cm on each side dispersed in anhydrous DMF (45 mL) and magnetically stirred for two hours. Chlorosulfonic acid was added dropwise to 5 mL of DMF chilled in an ice bath in quantities of 0.41, 0.51, or 0.62 mL, corresponding to 1.0, 1.25, or 1.5 moles of HSO_3Cl per mole of cellulose anhydroglucose units (AGU), respectively. Each of these acid/DMF mixtures (5 mL) was added to the dispersed cellulose (1 g in 45 mL DMF) to react at ambient temperature for 30, 45, or 60 min, respectively. The reaction was terminated by adding 10 mL purified water and centrifuging, followed by three additional rounds of washing *via* resuspension and centrifugation. The washed sulfated cellulose (SCell) was then dialyzed against purified water using regenerated cellulose dialysis membranes for approximately one week, until the conductivity of the dialyzing water plateaued.

Each dialyzed SCell was defibrillated into SCNF by blending (30 000 rpm, 30 min) using a high-speed blender (Vitamix 5200) in 5 min increments with cooldown periods to prevent excessive heating. For the most highly sulfated SCell (1.5 HSO_3Cl/AGU molar ratio, 60 min reaction time), a briefer 5 min blending was also performed. Each aqueous suspension was centrifuged (Eppendorf 5804R, 5000 rpm, 15 min) to collect the SCNF-containing supernatant. The yield of SCNF was determined by drying an aliquot of the supernatant to determine the concentration, multiplying by supernatant volume to get SCNF mass, and dividing this by the mass of purified SCell.

Characterization of SCNF

The degree of sulfation for each reaction condition was determined through conductometric titration. SCNF was diluted to below 0.2 wt% and run through a column packed with Dowex Marathon C acidic ion exchange beads to ensure that the sulfate half-ester groups were in their protonated form. The protonated SCNF was then titrated to the equivalence point with 0.01 M NaOH OAKTON pH meter (pH/Con 510 series). The level of sulfation (mmol g^{-1} of cellulose) is then equal to the moles of NaOH titrant utilized divided by the mass of SCNF.

Atomic force microscopy (AFM) was used to determine nanofibril height and length. Each aq. SCNF sample was diluted to *ca.* 0.0001 wt% and 10 μL was deposited on a freshly cleaved mica disc and allowed to dry. Samples were scanned using an Asylum Research MFP-3D AFM in tapping mode with OMCL-AC160TS standard silicon probes with a nominal tip radius of 7 nm and force constant of 26 N m^{-1}, 5 μm × 5 μm scan size in 512 × 512 pixels. The open-source software programs Gwyddion and ImageJ were utilized to determine the height and length of nanofibrils from collected scans.

Transmission electron microscopy (TEM) was used to determine the width of SCNF. A drop of SCNF dispersions at 0.01 wt% was deposited on glow-discharged TEM grids (300 mesh, coated with carbon/formvar) and blotted dry after 10 minutes. Samples were then repeatedly stained with 2 wt% uranyl acetate to enhance contrast. Micrographs were taken with a JEOL 2100F TEM equipped with a Schottky FEG electron source at an accelerating voltage of 200 kV. The widths of nanofibrils were determined using ImageJ. TEM micrographs for 30 min blended 2.23 mmol g^{-1} SCNF were unavailable, but widths are presumed similar to the 5 min blended sample of the same SCNF.

The crystallinity index (CrI) of SCNF and the dissolving pulp cellulose starting material were determined using X-ray diffraction (XRD). SCNF films approximately 10 μm thick were made by depositing approximately 10 mL of SCNF in a glass dish and drying it at 50 °C. The films were mounted on the stage of a Bruker D8 Advance Eco diffractometer with a Cu Kα radiation source using a very small amount of high-vacuum grease. Dissolving pulp cellulose was instead deposited on the stage as a powder, rather than being formed into a film. Scans were collected at 2θ values ranging from 5° to 40° with an angular increment of 0.03° and a scan time of 2.5 s per increment. Crystallinity was estimated from XRD using the Segal method.[23]

Aqueous exfoliation of graphite into graphene

SCNF and graphite flakes were mixed in aqueous media in varying ratios and high-speed blended, similar to a previously reported procedure applied to TEMPO oxidized CNF.[13] For optimization of blending conditions, two variables were examined: the aqueous graphite concentration and the graphite to SCNF mass ratio in the feed. Graphite concentrations of 5, 10, and 15 mg mL^{-1} and graphite/SCNF mass ratios of 2.5, 5, and 7.5 in the feed were used. All runs were done in duplicate with 5 runs for the center point. For a typical aqueous exfoliation run, SCNF was brought to neutral pH using NaOH. SCNF and graphite flakes were mixed, and water was added to reach a total volume of 100 mL. This mixture was blended (Vitamix 5200) at 37 000 RPM for 30 min in 10 min increments with cooldown periods between. After blending, the mixture was allowed to cool to room temperature then centrifuged (Eppendorf 5804R, 5000 rpm, 15 min) to precipitate unexfoliated graphite and collect the aqueous SCNF/graphene supernatant.

Simultaneous SCell defibrillation and graphite exfoliation was also studied, consolidating both blending steps into one. This process proceeded through a procedure analogous to the one detailed above for SCNF and graphite, with 10 mg mL^{-1} of aqueous graphite and a 5 graphite/SCell mass ratio in the feed.

Graphene characterization

The composition of each SCNF/graphene supernatant was determined through thermogravimetric analysis (TGA). Aliquots of the SCNF/graphene supernatants were dried at 50 °C and *ca.* 5 mg of each dried SCNF/graphene was tested using a Shimadzu TGA-50 in a nitrogen environment with a heating rate of 10 °C min^{-1} and max temperature of 500 °C. Quantitative analysis was performed using the free software package TRIOS (TA Instruments) by taking the first derivative of the TGA scan and integrating the primary SCNF decomposition peak, occurring at approximately 250 °C. As graphene shows no appreciable decomposition at this temperature,[13] the wt% of SCNF in each SCNF/graphene was estimated by dividing this integral by the integrated decomposition peak of SCNF alone.

The dimensions of exfoliated graphene were assessed using AFM. Drops of diluted SCNF/graphene suspension (0.0005 wt%) were deposited on mica and AFM imaging was carried out through an identical procedure to that highlighted for the analysis of SCNF. The height and lateral dimensions of the exfoliated graphene sheets were determined using Gwyddion. If a graphene sheet was rectangular or oblong shaped, the shorter lateral dimension was measured.

SCNF/graphene films were made through vacuum filtration. 25 mL of 0.1 wt% aqueous SCNF/graphene were filtered for 24 h using polycarbonate filters with a diameter of 47 mm and a 0.6 μm pore size. The film conductivity (σ) was determined by measuring the electrical resistance (R_s) using the four-point probe method[24] with colinear probes spaced 1 mm apart. The R_s was measured at several different locations on each film and averaged to calculate conductivity $\sigma = 1/(t\,R_s)$[25] using thickness (t) measured by a digital micrometer.

Results & discussion

SCNF characterization

Sulfation of dissolving pulp cellulose with chlorosulfonic acid in anhydrous DMF was conducted at HSO_3Cl/AGU molar ratios of 1.0, 1.25, and 1.5 and reaction times of 30, 45, and 60 min, respectively, to produce SCell with three distinct levels of sulfation or anionic charges of 1.48, 1.81, and 2.23 mmol g^{-1}. Blending these SCell samples for 30 minutes disintegrated nearly all into SCNF in 99.0, 99.0, and 99.9 wt% yields, respectively. The most highly sulfated SCNF (2.23 mmol g^{-1}) exhibited much shorter nanofibrillar lengths (365 nm) compared to the milder two SCNF (693 and 577 nm, respectively) when blended for 30 minutes (Fig. 1e). Therefore, an additional batch of 2.23 mmol g^{-1} SCNF was blended for only 5 minutes, producing longer nanofibers (501 nm long) more comparable to those from the milder two conditions (Fig. 1c). This much shorter blending time still converted an impressive 98.4% of SCell into SCNF—a testament to the efficacy of sulfation *via* chlorosulfonic acid pretreatment. While reaction and blending conditions were found to have a significant effect on nanofibril

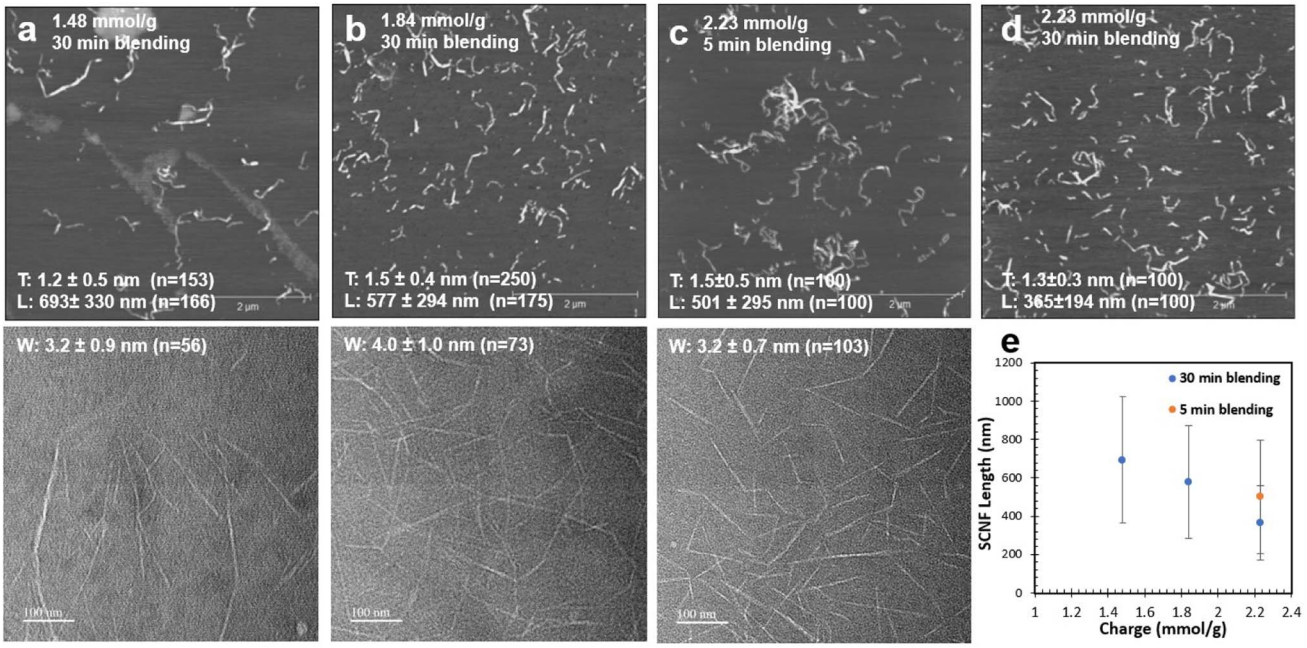

Fig. 1 AFM (top) and TEM (bottom) images of SCNF produced by sulfation reaction with chlorosulfonic acid under optimal conditions to varied charges of: (a) 1.48 mmol g^{-1} (1.0 HSO_3Cl/AGU, 30 min); (b) 1.84 mmol g^{-1} (1.25 HSO_3Cl/AGU, 45 min); (c and d) 2.23 mmol g^{-1} (1.5 HSO_3Cl/AGU, 60 min); (e) length *vs.* charge.

length, nanofibril thickness and width remained relatively similar across all HSO_3Cl/AGU molar ratios and reaction times, ranging narrowly from 1.2 to 1.5 nm and 3.2 to 4.0 nm, respectively (Fig. 1a–d). All SCNFs produced possess anisotropic cross sections, with width-to-thickness (W/T) ratios ranging from 2.1 to 2.7.

The combination of chlorosulfonic acid treatment and blending led to a reduction in the crystallinity index (CrI) of dissolving pulp cellulose. The original cellulose had a CrI of 0.81, while all four batches of SCNF had a CrI of around 0.65, irrespective of the sulfation or blending conditions studied, as observed by the overlap in the normalized XRD peaks for SCNF (Fig. 2a). This reduction in CrI suggests that sulfation not only affects cellulose in the amorphous regions but also amorphous–crystalline interfaces or crystalline surfaces.

As AFM was conducted on freshly cleaved hydrophilic mica surfaces, the SCNF surfaces in contact with the imaging surface are presumed to represent hydrophilic surfaces (110 or $1\bar{1}0$ crystalline planes), whereas the edges could represent hydrophobic surfaces (200 crystalline planes) of SCNF cross-sections (Fig. 2b). Applying this simplified SCNF cross-sectional model and known nanofibril dimensions, it can be estimated the SCNF are more hydrophilic, as evidenced by the 2.1–2.7 W/T ratios. Given that the width and thickness did not vary dramatically between sulfation and blending conditions, these SCNFs have similar overall hydrophilic–hydrophobic proportions on their surfaces. The main difference between SCNF batches lies in the density of charged sulfate half-ester groups present on the hydrophilic surfaces. Therefore, SCNF are expected to have similar ability to interact with graphene (*via* similar proportions of exposed hydrophobic planes) but may exhibit varied charge-dependent aqueous dispersibilities. This SCNF series also provides a range of well represented C6 sulfated CNFs along with C6 and C2/C3 carboxylated CNFs by respective TEMPO and periodate–chlorite oxidation of the same dissolving pulp[26] toward the development of a toolbox of safer by design substance evaluation tools linking the biological behavior of functionalized CNFs to their surface chemistries, charges, and dimensions.[27]

Aqueous exfoliation of graphite into graphene

To exfoliate graphite into graphene in aqueous media, SCNF is thought to play the dual roles of binding to the hydrophobic graphite surfaces *via* their hydrophobic surfaces and suspending the exfoliated graphene *via* their charged hydrophilic surfaces as demonstrated with TEMPO CNF.[13] For each SCNF tested, two experimental factors were varied when performing graphite exfoliation: the graphite concentration and the graphite/SCNF mass ratio in the initial feed. A two-level full factorial with five replicate center points (10 mg mL^{-1} graphite, 5 : 1 w/w graphite/SCNF) was conducted to assess the effect of each of the two variables of interest.

Using the least sulfated SCNF (1.48 mmol g; T: 1.2 nm, W: 3.2 nm; L: 693 nm), each aqueous mixture of graphite and SCNF was blended and then centrifuged to collect the supernatant containing the exfoliated graphene and the associated SCNF, with any un-exfoliated or large fragmented graphite remaining as precipitate. The first response examined was the graphene content in the graphene/SCNF supernatant. This serves as a measure of how efficiently SCNF could exfoliate and disperse graphene while also providing the graphene content in each

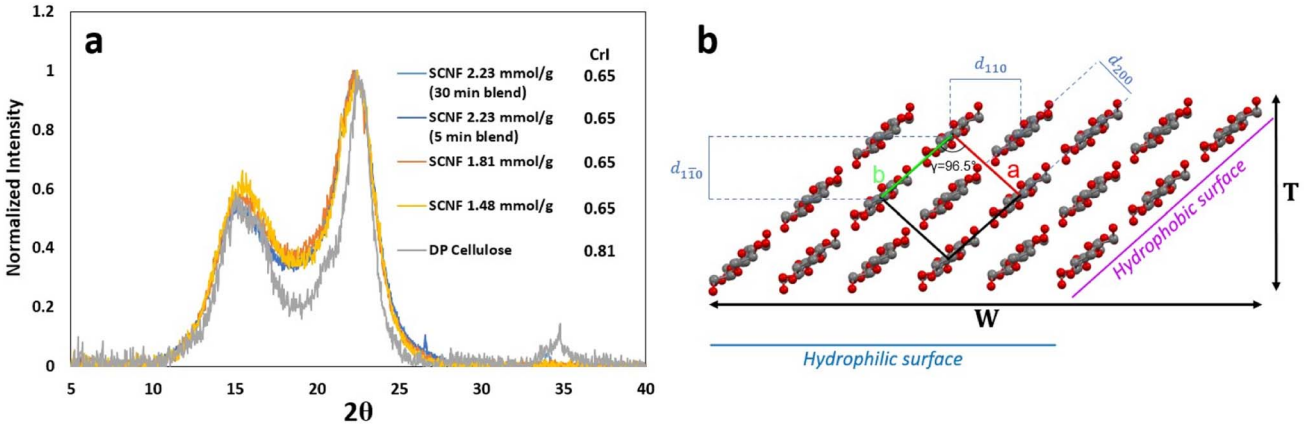

Fig. 2 SCNF: (a) crystallinity (CrI) by XRD; (b) cross-sectional model showing hydrophobic and hydrophilic crystalline planes.

graphene/SCNF dispersion. The second response of interest is the graphene yield, expressed as the wt% of graphene exfoliated from the starting graphite in the feed. The main effects plots (Fig. 3) show that the graphene content of the supernatant increased from 13.5 to 19.5 wt% as the graphite/SCNF feed ratio is increased from 2.5 to 5 initially, then leveled off at 19.6% with a further increase of graphite/SCNF feed ratio to 10 (Fig. 3a). At a 2.5 graphite/SCNF feed ratio, 4.8% graphite in the original feed was converted to graphene. The graphite to graphene conversion lowered to 3.9% and 2.1%, as the graphite/SCNF feed ratio increased from 2.5 to 5 and 7.5, respectively (Fig. 3a). This falls within expectations, as higher feed ratios see more graphite added to the system without any increase in SCNF.

The effect of aqueous graphite concentration on the graphene composition of the supernatant closely aligns with that of the graphite/SCNF feed ratio, with an initial increase in graphene content followed by a plateau (Fig. 3b). Interestingly, the conversion of graphite to graphene was improved by a small but statistically significant margin as graphite concentration was increased (Fig. 3b). The interaction plots for this experiment appear parallel, indicating no significant two-factor interaction between the graphite concentration and graphite/SCNF ratio variables (Fig. 4). Balancing both the graphene concentration in the supernatant and the graphite to graphene conversion, the optimal exfoliation condition for 1.48 mmol g^{-1} SCNF appeared to be a 5 : 1 graphite : SCNF feed ratio and a 10 mg mL^{-1} aqueous graphite concentration. These conditions led to the conversion of 3.9 ± 0.3 wt% of the starting graphite in the feed into graphene, with 19.5 ± 1.5 wt% of suspended solids being graphene.

Using the exfoliation conditions highlighted above, the effect of varying sulfated SCNFs on exfoliation was explored. At the 2.23 mmol g^{-1} level, the 5 minute blended sample was used to keep the nanofibrillar dimensions closer to the two lower charged SCNF. As SCNF charge increased from 1.48 to 1.81 and 2.23 mmol g^{-1}, less graphene was exfoliated and suspended, with the concentration of graphene in the supernatant falling

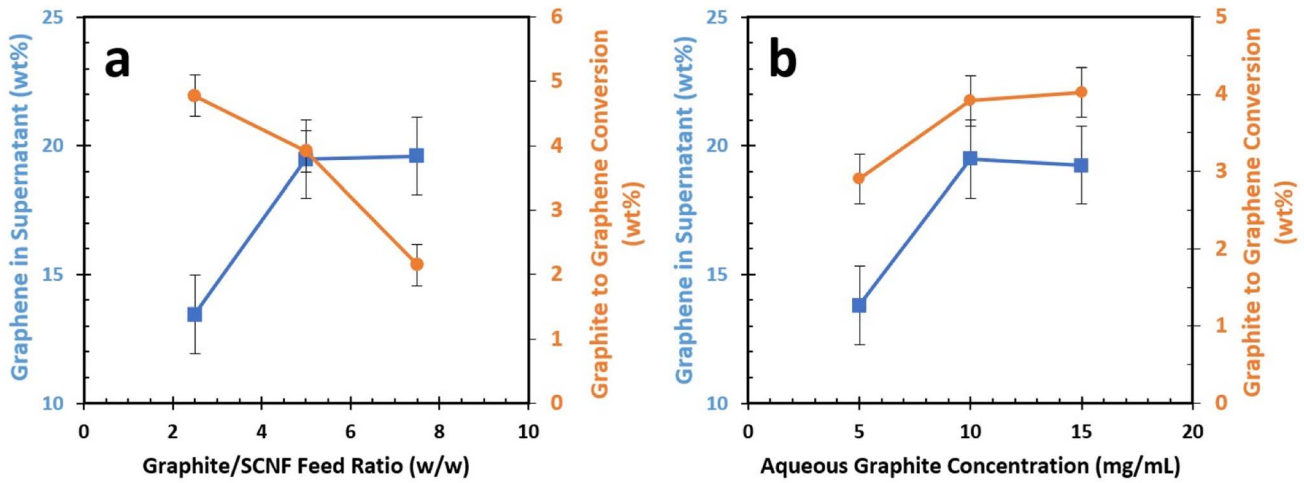

Fig. 3 Aqueous exfoliation of graphite to graphene in the presence of amphiphilic SCNF (1.48 mmol g; T: 1.2 nm, W: 3.2 nm; L: 693 nm): graphite/graphene conversion and wt% of graphene in the supernatant suspended solids as a function of (a) graphite/SCNF feed ratio; (b) initial graphite concentration.

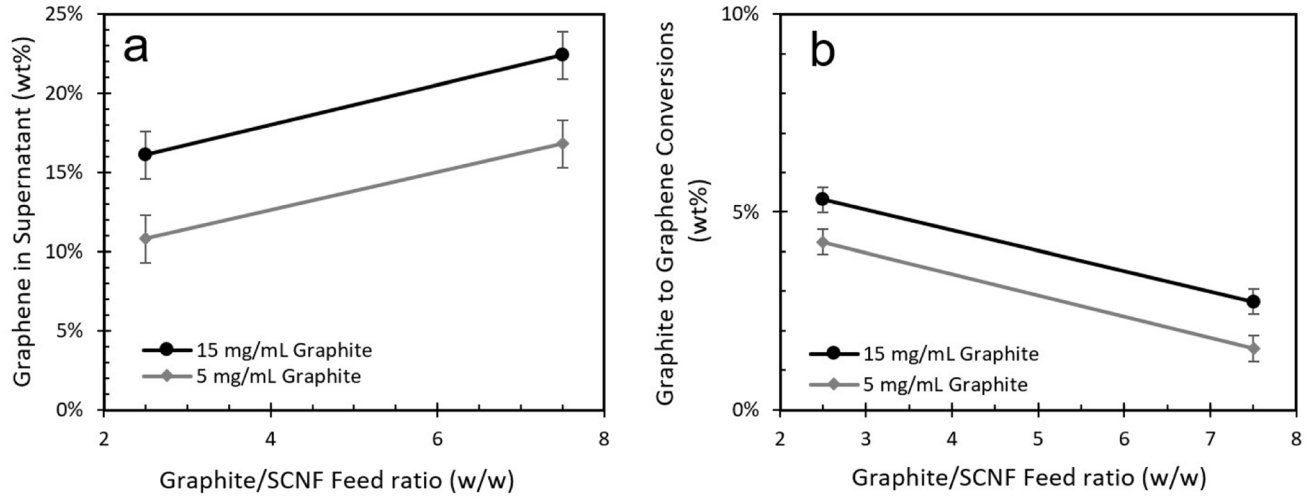

Fig. 4 Interaction plots showing the effect of varying graphite/SCNF feed ratio at different aqueous graphite concentrations on: (a) wt% of graphene in the supernatant suspended solids; (b) graphite to graphene conversion.

from 19.5 to 8.9 and 8.2 wt%, respectively (Fig. 5). As all three SCNF have similar width/thickness ratios or presumed proportions of hydrophobic-to-hydrophilic surfaces, the reduction in exfoliated/suspended graphene with increasing charge (hydrophilicity) may be taken as an indication that the hydrophobic interactions between graphene and SCNF were interfered by the increasing charges on the hydrophilic planes in this process.

Since both the defibrillation of sulfated cellulose (SCell) into SCNF and the exfoliation of graphite into graphene were carried out by the same shear force generated by high-speed blending and in aqueous media, the prospect of combining the two separate shearing processes into a single one-pot process was also examined. SCell was substituted for SCNF at the same conditions (10 mg mL^{-1} graphite, 5 : 1 feed ratio) for each charge level. It was found that the amount of graphite exfoliated increased as more highly charged SCell was utilized. Interestingly, this is the opposite trend compared to what was observed during the two separate defibrillation–exfoliation process when SCNF was utilized. In particular, the most charged 2.23 mmol g^{-1} SCell led to a much higher production of exfoliated graphene in the supernatant (12.2 wt%) than that by the two-step process (8.2 wt%) using SCNF with the same charge. It is reasonable to assume that the presence of graphite in the blending mixture may affect how SCell defibrillates into SCNF. Higher charged SCell may work better for this one-pot defibrillation–exfoliation due to the greater ease with which the SCell is defibrillated into SCNF. However, it is worth noting even the best forming one-pot trial with 2.23 mmol g^{-1} SCell still produced less graphene (12.2%, Fig. 5) than the *ca.* 19.5% graphene exfoliated under the same 5 : 1 feed ratio, 10 mg mL^{-1} graphite concentration utilizing 1.48 mmol g^{-1} SCNF (Fig. 3). While this process does save time and energy, it appears to come at the cost of lower efficiency. However, the robust sulfation and easy tuning of SCNF properties with this in mind may close this gap.

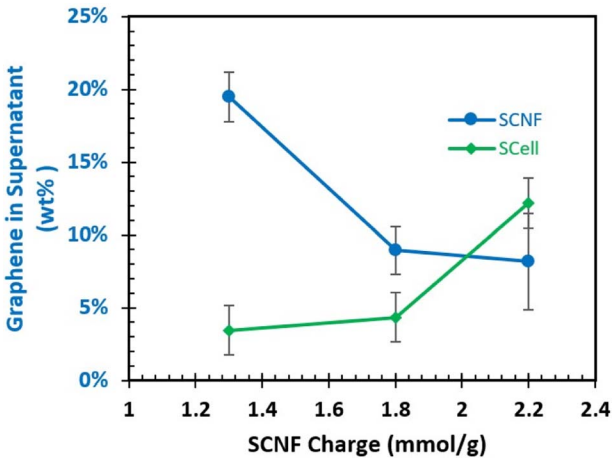

Fig. 5 Effect of sulfated cellulose or SCNF charges on graphene exfoliation efficacy.

Graphene quality

The thickness and lateral dimensions of graphene exfoliated from the graphene/SCNF dispersion that yielded the highest quantity of graphene in the supernatant (19.5 wt% graphene) using 1.48 mmol g^{-1} SCNF (T: 1.2 nm, W: 3.2 nm, L: 693 nm; 10 mg mL^{-1} graphite, 5 : 1 feed ratio) was further assessed. AFM of the dispersion shows visible graphene sheets amidst SCNF (Fig. 6a), with measured graphene sheet thickness ranging between 0.20 and 0.49 nm (Fig. 6b). Using the 0.335 nm monolayer thickness reported for graphene,[28] all the graphene observed consisted of either monolayer or bilayers. Since the distribution of graphene sheet thicknesses does not appear bimodal, the relative abundance of mono- and bilayers was determined by setting a threshold as the cutoff point. Taking a conservative estimate that monolayers should have an AFM measured thickness of no more than 0.335 nm leads to the

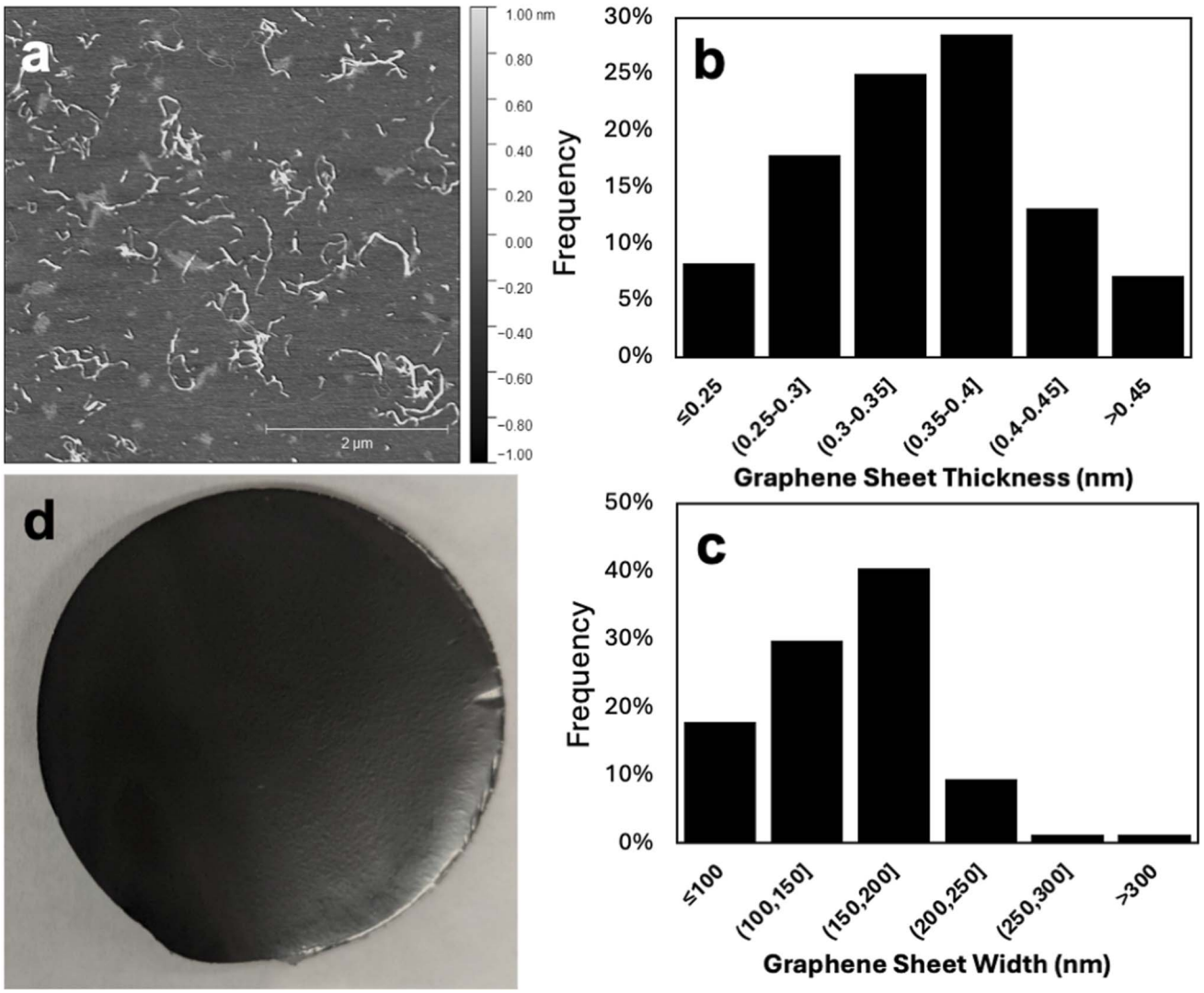

Fig. 6 Graphene/SCNF: (a) AFM height profile of aqueous dispersion (0.0001 wt%); (b) histogram of graphene sheet thickness; (c) histogram of graphene sheet width; (d) vacuum filtered graphene/SCNF film.

result that 42% of graphene sheets observed were monolayers, with the remaining 58% being bilayers. This result differs significantly from the layer distribution (determined by the same method) of graphene exfoliated using TEMPO CNF from rice straw (T: 1.7 nm, W: 2.6 nm; L: 990 nm), which consisted of approximately 5% monolayers, 19% bilayers, 26% triple layers, 47% with 4–9 layers, and 3% with 10+ layers.[13] A possible explanation for this phenomenon is that the hydrophobic interactions between (200) planes on SCNF and graphite may be weaker compared to TEMPO, either due to the difference in the relative lesser proportion of the hydrophobic (200) planes (2.6 *vs.* 1.5 W/T ratio for TEMPO) or in the charge nature or level (1.48 *vs.* 1.33 mmol g^{-1} for TEMPO). Weaker hydrophobic interactions or lesser SCNF-graphite affinity is thought to lead to a gentler exfoliation process, wherein only lighter mono- and bilayers could be removed from the bulk graphene flakes under the same shear force during high-speed blending. This finding is significant, as monolayer graphene is generally considered more desirable than multilayer samples. The width of graphene sheets ranged from 76 to 353 nm, with the highest fraction of sheets having widths on the order of 150–200 nm (Fig. 6c). This are similar to the lateral dimensions measured for graphene exfoliated by TEMPO CNF, which had average sheet widths of 248 ± 121 nm.[13] Even the finest of the sheets measured have widths many times larger than the radius of the AFM probe tip (nominally 7 nm), which means that height measurements of graphene sheets should be unaffected by the peak broadening and height reduction that is often observed when nanoscale features (such as SCNF themselves) are measured due to finite tip sharpness.[29]

The optimal graphene/SCNF dispersion with the highest 19.5 wt% graphene was vacuum fitrated to form free-standing films with an average thickness of 18.8 (±0.8) μm (Fig. 6d). The graphene/SCNF film showed moisture sensitivity, bending and curling when exposed to a humid environment and straightening again once in a lower humidity setting, similar to

films made from graphene/TEMPO CNF.[13] This behavior can be explained by the absorption of water molecules causing asymmetric expansion in SCNF on the side of the film exposed to moisture, leading to bending. The conductivity of the graphene/SCNF film was 0.60 ± 0.05 S cm^{-1}, much lower than the in-plane conductivity of graphene or even graphite due to the very large amount of the non-conducting SCNF (*ca.* 80 wt%) still present in the film. To improve electric conductivity of such graphene/SCNF films, SCNF may be removed by leveraging the significant differential thermal or chemical stability of graphene relative to SCNF. SCNF may be reduced or even removed thermally by pyrolysis or chemically *via* dissolution with solvents like *N*-methylmorpholine *N*-oxide (NMMO) and/or other chemical reactions that could degrade or depolymerize cellulose and allow for its removal from the system. Ultimately, the potential to improve graphene quality must be weighed against the additional processes or post treatments. At the same time, the presence of SCNF in the graphene dispersion permits viscosity control to offer novel processing opportunities such as fiber spinning into high strength fibers as previously demonstrated.[22] Furthermore, aqueous graphene/SCNF dispersions may be concentrated to increase viscosity or to form gel, allowing film formation or lamination by doctor blade coating.

Conclusion

Sulfated cellulose nanofibrils with sulfation levels of 1.48, 1.81, and 2.23 mmol g^{-1} were produced from dissolving pulp cellulose with a combination of chlorosulfonic acid treatment and high speed blending. SCNF produced had similar widths and thicknesses irrespective of reaction conditions, but length was found to decrease with increasing level of sulfation and length of blending. SCNF with 1.48 mmol g^{-1} of sulfate groups was found to be effective to exfoliate graphite into graphene, under the optimal condition of 5 graphite-to-SCNF w/w ratio with 10 mg mL^{-1} graphite in the original feed. This converted 3.9% of graphite to graphene and yielded 19.5 wt% graphene in the suspended solids. The aqueously exfoliated graphene appeared to consist exclusively of monolayers and bilayers with 42% monolayers; a greater abundance of much thinner layers than when using TEMPO-oxidized CNF. Furthermore, it was possible to combine the two separate defibrillation of sulfated cellulose and the exfoliation of graphite into one single blending step for simultaneous production of SCNF and graphene, saving significant time and energy. While this one-pot simultaneous process produced less graphene than the two discreet blending steps with less sulfated cellulose, it was found to improve at higher cellulose sulfation levels and further tuning of SCNFs with the robust sulfation has the potential to become an effective and efficient strategy.

Author contributions

Conceptualization, data curation, formal analysis, investigation, methodology, BP, YLH; funding acquisition, JDE, CMS, JAS, NS, YLH; project administration, JDE, JAS, YLH; supervision, YLH; visualization, BP, YLH; writing – original draft, BP, YLH; writing – review & editing, BP, JDE, CMS, JAS, NS, YLH.

Conflicts of interest

The authors declare no competing financial interest.

Acknowledgements

The financial support from P3 Nano and the United States Department of Defense's Science, Mathematics, and Research for Transformation (SMART) scholarship is greatly appreciated. Part of this study was carried out at the UC Davis Center for Nano and Micro Manufacturing (CNM2).

References

1 M. J. Allen, V. C. Tung and R. B. Kaner, Honeycomb Carbon: A Review of Graphene, *Chem. Rev.*, 2010, **110**(1), 132–145, DOI: 10.1021/cr900070d.
2 C. Lee, X. Wei, J. W. Kysar and J. Hone, Measurement of the Elastic Properties and Intrinsic Strength of Monolayer Graphene, *Science*, 2008, **321**(July), 385–388.
3 R. Ruoff, Calling All Chemists, *Nat. Nanotechnol.*, 2008, **3**(1), 10–11, DOI: 10.1038/nnano.2007.432.
4 L. Zhang, S. Zaric, X. Tu, X. Wang, W. Zhao and H. Dai, Assessment of Chemically Separated Carbon Nanotubes for Nanoelectronics, *J. Am. Chem. Soc.*, 2008, **130**(8), 2686–2691, DOI: 10.1021/ja7106492.
5 K. R. Paton, E. Varrla, C. Backes, R. J. Smith, U. Khan, A. O'Neill, C. Boland, M. Lotya, O. M. Istrate, P. King, T. Higgins, S. Barwich, P. May, P. Puczkarski, I. Ahmed, M. Moebius, H. Pettersson, E. Long, J. Coelho, S. E. O'Brien, E. K. McGuire, B. M. Sanchez, G. S. Duesberg, N. McEvoy, T. J. Pennycook, C. Downing, A. Crossley, V. Nicolosi and J. N. Coleman, Scalable Production of Large Quantities of Defect-Free Few-Layer Graphene by Shear Exfoliation in Liquids, *Nat. Mater.*, 2014, **13**(6), 624–630, DOI: 10.1038/nmat3944.
6 J. N. Coleman, Liquid Exfoliation of Defect-Free Graphene, *Acc. Chem. Res.*, 2013, **46**(1), 14–22, DOI: 10.1021/ar300009f.
7 S. Stankovich, R. D. Piner, X. Chen, N. Wu, S. T. Nguyen and R. S. Ruoff, Stable Aqueous Dispersions of Graphitic Nanoplatelets via the Reduction of Exfoliated Graphite Oxide in the Presence of Poly(Sodium 4-Styrenesulfonate), *J. Mater. Chem.*, 2006, **16**(2), 155–158, DOI: 10.1039/b512799h.
8 J. Geng, B. S. Kong, S. B. Yang and H. T. Jung, Preparation of Graphene Relying on Porphyrin Exfoliation of Graphite, *Chem. Commun.*, 2010, **46**(28), 5091–5093, DOI: 10.1039/c001609h.
9 X. Xu, J. Zhou, V. Colombo, Y. Xin, R. Tao and G. Lubineau, Sodium Hypochlorite and Sodium Bromide Individualized and Stabilized Carbon Nanotubes in Water, *Langmuir*, 2017, **33**(41), 10868–10876, DOI: 10.1021/acs.langmuir.7b00850.

10 Y. Xu, H. Bai, G. Lu, C. Li and G. Shi, Flexible Graphene Films via the Filtration of Water-Soluble Noncovalent Functionalized Graphene Sheets, *J. Am. Chem. Soc.*, 2008, **130**(18), 5856–5857, DOI: **10.1021/ja800745y**.

11 C. A. Furtado, U. J. Kim, H. R. Gutierrez, L. Pan, E. C. Dickey and P. C. Eklund, Debundling and Dissolution of Single-Walled Carbon Nanotubes in Amide Solvents, *J. Am. Chem. Soc.*, 2004, **126**(19), 6095–6105, DOI: **10.1021/ja039588a**.

12 F. Jiang and Y.-L. Hsieh, Amphiphilic Superabsorbent Cellulose Nanofibril Aerogels, *J. Mater. Chem. A*, 2014, **2**(18), 6337–6342, DOI: **10.1039/c4ta00743c**.

13 X. Xu and Y. L. Hsieh, Aqueous Exfoliated Graphene by Amphiphilic Nanocellulose and Its Application in Moisture-Responsive Foldable Actuators, *Nanoscale*, 2019, **11**(24), 11719–11729, DOI: **10.1039/c9nr01602c**.

14 R. T. Shet, R. R. Wallajapet and P. Sulfonated, *Cellulose Having Improved Absorbent Properties*, *US Pat.*, US5703225A, 1995, **https://patentimages.storage.googleapis.com/12/25/8d/3bff3d2857e238/US5703225.pdf%0Ahttps://patents.google.com/patent/US5703225A/en**, (accessed 2019-01-10).

15 Q. X. Hou, W. Liu, Z. H. Liu and L. L. Bai, Characteristics of Wood Cellulose Fibers Treated with Periodate and Bisulfite, *Ind. Eng. Chem. Res.*, 2007, **46**, 7830–7837, DOI: **10.1021/ie0704750**.

16 H. Liimatainen, M. Visanko, J. Sirviö, O. Hormi and J. Niinimäki, Sulfonated Cellulose Nanofibrils Obtained from Wood Pulp through Regioselective Oxidative Bisulfite Pre-treatment, *Cellulose*, 2013, **20**, 741–749, DOI: **10.1007/s10570-013-9865-y**.

17 T. E. Nikiforova and V. A. Kozlov, Study of the Effect of Oxidative-bisulfite Modification of the Cotton Cellulose on Its Ion Exchange Properties, *Russ. J. Gen. Chem.*, 2011, **81**, 2136–2141, DOI: **10.1134/S1070363211100173**.

18 J. Zhang, N. Jiang, Z. Dang, T. J. Elder and A. J. Ragauskas, Oxidation and Sulfonation of Cellulosics, *Cellulose*, 2008, **15**, 489–496, DOI: **10.1007/s10570-007-9193-1**.

19 J. Luo, N. Semenikhin, H. Chang, R. J. Moon and S. Kumar, Post-sulfonation of Cellulose Nanofibrils with a One-step Reaction to Improve Dispersibility, *Carbohydr. Polym.*, 2018, **181**, 247–255. **https://www.sciencedirect.com/science/article/abs/pii/S014486171731233X**.

20 M. Horikawa, T. Fujiki, T. Shirosak, N. Ryu, S. Nagaoka and H. Ihara, The Development of a Highly Conductive PEDOT System by Doping with Partially Crystalline Sulfated Cellulose and its Eelectric Conductivity, *J. Mater. Chem. C*, 2015, **3**, 8881–8887. **https://pubs.rsc.org/en/content/articlelanding/2015/tc/c5tc02074c**.

21 J. A. Sirviö, J. Ukkola and H. Liimatainen, Direct Sulfation of Cellulose Fibers using a Reactive Deep Eutectic Solvent to Produce Highly Charged Cellulose Nanofibers, *Cellulose*, 2019, **26**, 2303–2316, DOI: **10.1007/s10570-019-02257-8**.

22 B. Pingrey and Y.-L. Hsieh, Sulfated Cellulose Nanofibrils from Chlorosulfonic Acid Treatment and Their Wet Spinning into High-Strength Fibers, *Biomacromolecules*, 2022, **23**(3), 1269–1277, DOI: **10.1021/acs.biomac.1c01505**.

23 L. Segal, J. J. Creely, A. E. Martin and C. M. Conrad, An Empirical Method for Estimating the Degree of Crystallinity of Native Cellulose Using the X-Ray Diffractometer, *Text. Res. J.*, 1959, **29**(10), 786–794, DOI: **10.1177/004051755902901003**.

24 I. Miccoli, F. Edler, H. Pfnür and C. Tegenkamp, The 100th Anniversary of the Four-Point Probe Technique: The Role of Probe Geometries in Isotropic and Anisotropic Systems, *J. Phys.: Condens.Matter*, 2015, **27**(22), 220201, DOI: **10.1088/0953-8984/27/22/223201**.

25 J. Zhou and Y.-L. Hsieh, Conductive Polymer Protonated Nanocellulose Aerogels for Tunable and Linearly Responsive Strain Sensors, *ACS Appl. Mater. Interfaces*, 2018, **10**(33), 27902–27910, DOI: **10.1021/acsami.8b10239**.

26 M. Guo, J. D. Ede, C. M. Sayes, J. A. Shatkin, N. Stark and Y.-L. Hsieh, Regio-selective Carboxylated Cellulose Nanofibril Models from Dissolving Pulp: C6 via TEMPO-mediated Oxidation and C2,C3 via Periodate-chlorite Oxidation, *Nanomaterials*, 2024, **14**, 479. **https://www.mdpi.com/2079-4991/14/5/479**.

27 A. K. Charlton-Sevcik, C. Collom, J. Y. Liu, Y.-L. Hsieh, N. Stark, J. D. Ede, J. A. Shatkin and C. M. Sayes, The Impact of Surface Functionalization of Cellulose Following Simulated Digestion and Gastrointestinal Cell-based Model Exposure, *Int. J. Biol. Macromol.*in review.

28 Z. H. Ni, H. M. Wang, J. Kasim, H. M. Fan, T. Yu, Y. H. Wu, Y. P. Feng and Z. X. Shen, Graphene Thickness Determination Using Reflection and Contrast Spectroscopy, *Nano Lett.*, 2007, **7**(9), 2758–2763, DOI: **10.1021/nl071254m**.

29 S. Santos, V. Barcons, H. K. Christenson, J. Font and N. H. Thomson, The Intrinsic Resolution Limit in the Atomic Force Microscope: Implications for Heights of Nano-Scale Features, *PLoS One*, 2011, **6**(8), e23821, DOI: **10.1371/journal.pone.0023821**.